2011 American Control Conference
on O'Farrell Street, San Francisco, CA, USA
June 29 - July 01, 2011

Energy-Efficient Control Allocation with Applications on Planar Motion Control of Electric Ground Vehicles

Yan Chen and Junmin Wang*
Department of Mechanical and Aerospace Engineering
The Ohio State University
Columbus, OH 43210

Abstract—**This paper presents a control method for tracking electric ground vehicle planar motions while achieving the optimal energy consumption. Sliding mode control and an energy-efficient control allocation (CA) scheme are synthesized to track the desired vehicle longitudinal, lateral, and yaw motions. By explicitly incorporating actuator efficiencies and actuator operating modes into the coordination of redundant in-wheel motors equipped on electric ground vehicles, vehicle planar motion control and operating energy optimization are achieved simultaneously. Different maneuvers are tested for comparisons between the standard and the energy-efficient CA schemes. Based on experimental data and some reasonable assumptions on the efficiencies of in-wheel motors, the energy-efficient CA dictates different torque distributions on all the wheels under consideration of different efficiencies. Simulation results indicate that, in comparison to the results by the standard CA scheme, less energy is consumed when the energy-efficient CA scheme is applied for controlling the electric ground vehicle planar motions.**

I. Introduction

With the explosion of related technologies, such as high energy-density and/or power-density batteries, high-efficiency electrical machines, and high-performance energy management systems, electrical ground vehicles (EGV) have entered a fast developing stage recently. Within various EGV structures, EGVs actuated by in-wheel motors have attracted increasing interests from both industrial and academic communities due to the characteristics of higher control flexibility and further improvement on energy conversion. The mature in-wheel motor technology allows fast and accurate torque control for each of the EGV wheels [1][2]. The corresponding concept cars with independently-actuated in-wheel motors, such as the GM S10 Mule [3] and UOT electric March [4], have already proceeded into the prototyping and/or pre-market phases.

Compared with the conventional vehicle drivetrain architectures where driving and braking actions of different wheels are coupled, one salient advantage of EGVs with independently-actuated in-wheel motors is the higher control flexibility and consequently other potentials [5]-[7][30]. Four independently-actuated in-wheel motors formally make an EGV become an over-actuated system, in which the number of actuators is greater than the degrees of freedom [8][9]. Although early studies on over-actuated systems oriented from airplanes [14][15] and marine vessels [13], many developed methods, such as various control allocation algorithms, have already been recently applied to ground vehicles [16]-[18].

Control allocation (CA) is commonly employed in over-actuated systems to optimally allocate the desired virtual controls among all the available actuators within their respective constraints [5][6][10]-[12]. Although various CA methods have different limitations and strengths, numerical optimization-based CA algorithms are widely used in ground vehicles [16]-[20]. For a linearized yaw rate and sideslip angle model, Plumlee *et. al.* [17] applied quadratic programming based CA to track a desired yaw rate trajectory while minimizing the vehicle sideslip. Wang *et. al.* [18] proposed an accelerated fixed-point algorithm to solve quadratic programming CA, which was adopted for advanced coordinated vehicle dynamic control under considerations of vehicle operating condition and tire-road friction coefficient. Gerard and Verhaegen [16] suggested a two-layer global and local chassis control method based on tire force allocation, in which the force values were not necessarily optimized at each time step but trended fast enough in the optimal direction. Tjønnås and Johansen [19] applied an adaptive brake CA algorithm to fulfill the yaw stabilization of an automotive vehicle in extreme maneuvers. Moreover, Tagesson *et al.* [20] evaluated and compared the real-time performance of two popular numerical algorithms, active-set and primal-dual interior point when CA was applied to the yaw motion stability control of heavy vehicles.

Although different vehicle performances were achieved by various optimization-based CA methods within the aforementioned vehicle applications, the utilized CA algorithms rarely considered the energy optimization during virtual control effort distributions. Since minimizing the amplitudes of actuators in the CA algorithms does not necessarily lead to less power consumption due to the actuator efficiency characteristics, the authors preliminarily proposed an energy-efficient CA method to achieve energy optimization as well as vehicle longitudinal speed tracking [21]. This paper extends the energy-efficient CA to planar motion control of an EGV with a nonlinear control-oriented vehicle model and a high-level robust SMC. Moreover, based on experimental data and reasonable scaling factors on efficiencies of four in-wheel motors, different torque distributions, compared with the ones of the standard CA method, are obtained for achieving EGV planar motion control and optimal energy consumptions simultaneously.

The remainder of this paper is organized as follows. In

*Corresponding author. Authors' emails: chen.1843@osu.edu and wang.1381@osu.edu. This research was supported by the Office of Naval Research Young Investigator Award under Grant N00014-09-1-1018, Honda-OSU Partnership Program, and OSU Transportation Research Endowment Program.

section II, vehicle and tire dynamics for planar motions are introduced. A control-oriented model is also suggested. The high-level sliding mode controller and the low-level energy-efficient CA are described in section III. In section IV, co-simulations with Simulink/Matlab and CarSim are applied for different maneuvers in order to verify the energy saving of the energy-efficient CA during planar motion control. Conclusive remarks are presented in section V.

II. VEHICLE AND TIRE DYNAMICS

In this section, the control-oriented model for EGV planar motions is first introduced.

A. EGV control-oriented model for planar motions

Ground vehicles can be simply modeled as a rigid body with three degrees of freedom. Figure 1 shows the EGV planar dynamic motions (longitudinal, lateral, and yaw).

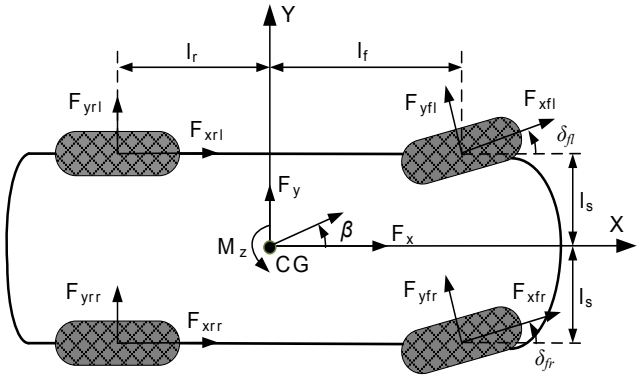

Figure 1. Ground vehicle planar dynamic motion.

The simplified vehicle planar dynamic equations of motion is written as

$$\begin{aligned} m_v(\dot{V}_x - rV_y) &= F_x - C_a V_x^2 \\ m_v(\dot{V}_y + rV_x) &= F_y \\ I_z\dot{r} &= M_z \end{aligned}, \quad (1)$$

where m_v is the vehicle mass (including both sprung and unsprung masses), V_x is vehicle velocity along the X axis, V_y is vehicle velocity along the Y axis, $r = \dot{\beta}$ is the vehicle yaw rate, and I_z is vehicle moment of inertia about the Z axis, which is perpendicular to the X-Y plane. The coordinates X, Y, Z are body-fixed at the vehicle center of gravity (CG). The generalized external forces acting along the vehicle X and Y axes are F_x and F_y, respectively. The generalized external moment about the Z axis is M_z. C_a is the aerodynamic resistance coefficient in the longitudinal direction. The wheelbase is represented by the sum of l_f and l_r. The track is shown as $2l_s$.

With in-wheel motors, each of the four wheels can independently drive or brake. Thus, these generalized forces/moment are expressed as [5],

$$\begin{aligned} F_x = {} & F_{xfl}\cos\delta_{fl} - F_{yfl}\sin\delta_{fl} + F_{xfr}\cos\delta_{fr} \\ & - F_{yfr}\sin\delta_{fr} + F_{xrl} + F_{xrr}, \end{aligned} \quad (2)$$

$$\begin{aligned} F_y = {} & F_{xfl}\sin\delta_{fl} + F_{yfl}\cos\delta_{fl} + F_{xfr}\sin\delta_{fr} \\ & + F_{yfr}\cos\delta_{fr} + F_{yrl} + F_{yrr}, \end{aligned} \quad (3)$$

$$\begin{aligned} M_z = {} & l_s\big(-F_{xfl}\cos\delta_{fl} + F_{yfl}\sin\delta_{fl} - F_{xrl} \\ & + F_{xfr}\cos\delta_{fr} - F_{yfr}\sin\delta_{fr} + F_{xrr}\big) \\ & + l_f\big(F_{xfl}\sin\delta_{fl} + F_{yfl}\cos\delta_{fl} \\ & + F_{xfr}\sin\delta_{fr} + F_{yfr}\cos\delta_{fr}\big) \\ & + l_r\big(-F_{yrl} - F_{yrr}\big). \end{aligned} \quad (4)$$

In these above relations, the wheel steering angles δ_{fl} (the inner wheel) and δ_{fr}(the outer wheel) satisfy the following Ackerman condition [28].

$$\cot\delta_{fr} - \cot\delta_{fl} = \frac{2l_s}{l_r + l_f}. \quad (5)$$

Moreover, the relationship between the vehicle steering angle δ and the wheel steering angles is given by

$$\cot\delta = \frac{\cot\delta_{fr} + \cot\delta_{fl}}{2}. \quad (6)$$

The rotational dynamics of each in-wheel motor is represented by

$$J\dot{\omega}_i = T_i - F_{xi}R_{eff}, \quad (7)$$

where the rotational inertia J and the effective radius R_{eff} of each wheel are assumed the same. The subscript $i \in \{fl, fr, rl, rr\}$ represents different in-wheel motor. Note that the output torque of each in-wheel motor T_i is positive during driving and negative during braking, respectively.

Let $x_1 = V_x$, $x_2 = V_y$, and $x_3 = r$, the following nonlinear control-oriented model for EGV planar motions is obtained by integrating equations (1)-(4) and (7) together.

$$\begin{aligned} \dot{x}_1 &= x_2x_3 - \frac{C_a}{m_v}x_1^2 + \frac{1}{m_v}\left(\frac{-J}{R_{eff}}\Delta_{1x}\dot{\omega} + \Delta_{1y}F_Y\right) + v_1 \\ \dot{x}_2 &= -x_1x_3 + \frac{1}{m_v}\left(\frac{-J}{R_{eff}}\Delta_{2x}\dot{\omega} + \Delta_{2y}F_Y\right) + v_2 \\ \dot{x}_3 &= \frac{1}{I_z}\left(\frac{-J}{R_{eff}}\Delta_{3x}\dot{\omega} + \Delta_{3y}F_Y\right) + v_3 \end{aligned}, \quad (8)$$

where

$F_Y = [F_{yfl} \quad F_{yfr} \quad F_{yrl} \quad F_{yrr}]^T$,

$\dot{\omega} = [\dot{\omega}_{fl} \quad \dot{\omega}_{fr} \quad \dot{\omega}_{rl} \quad \dot{\omega}_{rr}]^T$,

$\Delta_{1x} = [\cos\delta_{fl} \quad \cos\delta_{fr} \quad 1 \quad 1]$,

$\Delta_{1y} = [-\sin\delta_{fl} \quad -\sin\delta_{fr} \quad 0 \quad 0]$,

$\Delta_{2x} = [\sin\delta_{fl} \quad \sin\delta_{fr} \quad 0 \quad 0]$,

$\Delta_{2y} = [\cos\delta_{fl} \quad \cos\delta_{fr} \quad 1 \quad 1]$,

$\Delta_{3x} = \left[l_f\sin\delta_{fl} - l_s\cos\delta_{fl} \quad l_s\cos\delta_{fr} + l_f\sin\delta_{fr} \quad -l_s \quad l_s\right]$,

$\Delta_{3y} = \left[l_s\sin\delta_{fl} + l_f\cos\delta_{fl} \quad l_f\cos\delta_{fr} - l_s\sin\delta_{fr} \quad -l_r \quad -l_r\right]$.

Moreover, the virtual control v_d is expressed as

$$v_d = \begin{pmatrix} v_1 \\ v_2 \\ v_3 \end{pmatrix} = Bu, \quad (9)$$

with

$$B = \left[\frac{1}{m_vR_{eff}}\Delta_{1x}^T \quad \frac{1}{m_vR_{eff}}\Delta_{2x}^T \quad \frac{1}{I_zR_{eff}}\Delta_{3x}^T\right]^T,$$

$u = [T_{fl} \quad T_{fr} \quad T_{rl} \quad T_{rr}]^T$.

The wheel center speed in the direction of the tire heading is expressed

$$V_{fl} = (V_x - rl_s)\cos\delta_{fl} + \left(V_y + rl_f\right)\sin\delta_{fl}, \quad (10)$$

$$V_{fr} = (V_x + rl_s)\cos\delta_{fr} + \left(V_y + rl_f\right)\sin\delta_{fr}, \quad (11)$$

$$V_{rl} = V_x - rl_s, \quad (12)$$

$$V_{rr} = V_x + rl_s. \quad (13)$$

B. Tire model

One of the most well-known tire model is the "Magic Formula" tire model developed by Pacejka *et al.* [23], which is generally accepted as a fairly accurate model and widely adopted in vehicle dynamical simulations and analysis [24][25][28]. The basic equations of the Pacejka model are

$$\begin{aligned} y(x) &= D\sin\{C\tan^{-1}[Bx - E(Bx - \tan^{-1}Bx)]\} \\ Y(X) &= y(x) + S_v \\ x &= X + S_h \end{aligned} \quad (14)$$

Within this equation, $Y(X)$ represents tire longitudinal force, lateral force or self-aligning moment. X is tire slip ratio or slip angle. C is the shape factor, D is the peak factor, B is the tire stiffness factor, E is the curvature factor. S_v and S_h denote the vertical shift and the horizontal shift, respectively. All these coefficients are tuned to fit experimental data for a given tire on a test patch. The model coefficients in this paper are taken from references [5][6].

III. High-level control design and energy-efficient control allocation

In order to track desired planar motions, the hierarchical control strategy consisting of a high-level sliding mode controller (SMC) and a low-level energy-efficient CA algorithm is adopted. The SMC offers the generalized forces/moments required to track the desired planar vehicle motions. The energy-efficient CA algorithm distributes the generalized actuation to each wheel in an optimal energy consumption way according to different motor efficiencies.

A. High-level sliding mode controller design

For vehicle tracking control, a SMC is designed to accommodate the uncertainties involved in vehicle dynamics. For the control-oriented model (8), the SMC design is partitioned into three single-input single-output (SISO) systems since the control input are decoupled. Followed the standard design procedure of SMC in [7][26][27], the three virtual control signals are directly displayed in the following.

$$\begin{aligned} v_1 = \frac{C_a}{m_v}x_1^2 - x_2x_3 - \frac{1}{m_v}\left(\frac{-J}{R_{eff}}\Delta_{1x}\dot{\omega} + \Delta_{1y}\hat{F}_Y\right) + \dot{x}_{1r} \\ - k_1\mathrm{sign}(s_1), \end{aligned} \quad (15)$$

$$\begin{aligned} v_2 = x_1x_3 - \frac{1}{m_v}\left(\frac{-J}{R_{eff}}\Delta_{2x}\dot{\omega} + \Delta_{2y}\hat{F}_Y\right) + \dot{x}_{2r} \\ - k_2\mathrm{sign}(s_2), \end{aligned} \quad (16)$$

$$v_3 = -\frac{1}{I_z}\left(\frac{-J}{R_{eff}}\Delta_{3x}\dot{\omega} + \Delta_{3y}\hat{F}_Y\right) + \dot{x}_{3r} - k_3\mathrm{sign}(s_3). \quad (17)$$

Within the above equations, the control gain $k_j > 0$ $(j = 1,2,3)$ can be appropriately chosen to address the parameter uncertainties. x_{jr} represents the reference longitudinal, lateral speed and yaw rate, respectively. The estimated lateral friction force $\hat{F}_Y$ is calculated based on the Magic Formula tire model (14). Angular acceleration $\dot{\omega}$ can be approximately calculated by measured angular velocity signals.

One potential problem for the control law (17) is that the yaw rate error caused in the chattering effect of SMC design could accumulate to an offset on the yaw angle and consequently lead to a vehicle heading deviation. Adding a new control of yaw angle, an integral state of yaw rate, can resolve this problem in the later simulation. Let $x_4 = \beta$, the virtual control v_3 is redesigned for the following double –integrator system.

$$\begin{aligned} \dot{x}_3 &= \frac{1}{I_z}\left(\frac{-J}{R_{eff}}\Delta_{3x}\dot{\omega} + \Delta_{3y}F_Y\right) + v_3, \\ \dot{x}_4 &= x_3. \end{aligned}$$

Define $S_3 = x_3 - x_{3r} + \lambda_4(x_4 - x_{4r})$, where x_{4r} is the desired yaw angle by integrating x_{3r} over time and $\lambda_4 > 0$ is the parameter of sliding surfaces. Following the similar SMC design procedure, the control law (17) is modified as

$$\begin{aligned} v_3 = -\frac{1}{I_z}\left(\frac{-J}{R_{eff}}\Delta_{3x}\dot{\omega} + \Delta_{3y}\hat{F}_Y\right) - \lambda_4(x_3 - x_{3r}) \\ + \dot{x}_{3r} - k_3\mathrm{sign}(s_3). \end{aligned} \quad (18)$$

Thus, the control laws shown in (15), (16) and (18) ensure that the EGV planar motions tracking.

To reduce chattering effects in practical implementation of the control laws, $\mathrm{sign}(\cdot)$ function is approximately replaced by a saturation function [26][27].

$$\mathrm{sign}(s_i) \approx \mathrm{sat}\left(\frac{s_i}{\Phi_i}\right) \quad (19)$$

where Φ_i is the boundary layer thickness around the sliding surface s_i. The selection of the thickness of the boundary layer Φ_i is a tradeoff between reducing the chattering effect and increasing residual error.

B. Energy-efficient control allocation

The energy-efficient CA scheme [21] is applied to the tracking control of planar motions. Since all the four in-wheel motors can independently drive and brake and the dual-mode energy-efficient CA actually contains the single-mode algorithm, the dual-mode CA is adopted here. Based on the virtual control expression (9), the dual-mode energy-efficient CA is represented as,

$$\begin{aligned} &\min\ J = \|W_v(B_a[u^T \quad u'^T]^T - v_d)\| + \lambda P_c, \\ &\text{s.t.} \begin{cases} u_{min} \le u \le u_{max} \\ u'_{min} \le u' \le u'_{max} \\ u_i u'_i = 0,\ i \in \{fl, fr, rl, rr\} \end{cases} \end{aligned} \quad (20)$$

where the virtual actuators $u' = [T'_{fl} \quad T'_{fr} \quad T'_{rl} \quad T'_{rr}]^T$ stand for the regenerative brake torques. Since the equation (7) has the same expressions for both driving and braking except the sign of torque is opposite, the control effectiveness matrix $B_a = [B \quad B]$. W_v and λ are the weighting matrix and optimization scaling factor, respectively. The above constraints apply to the real and virtual actuators component-wisely.

Within equation (20), the total power consumption of the four in-wheel motors in different modes is formulated as

$$P_c = \sum_i \frac{P_{oi}(u_i)}{\eta_{oi}(u_i)} - \sum_i P_{ii}(u'_i)\eta_{ii}(u'_i). \quad (21)$$

Here, P_{oi} denotes the output power at the energy consuming mode and P_{ii} is the input power at the energy gaining mode. The actuator efficiencies at energy consuming and gaining modes are represented by η_{oi} and η_{ii}, respectively. The energy gaining actuation mode is inferred by the minus sign in front of virtual actuator power consumption. For in-wheel motors in EGV, the power consumption expressions are

formulated as [21],

$$P_{oi}(T_i) = T_i\omega_i(T_i) = \frac{T_i^2 + KR_{eff}T_i}{KR_{eff}^2}V_i. \quad (22)$$

where K is the tire longitudinal stiffness and V_i is the wheel center speed shown in (10)-(13). The input power $P_{ii}(T'_i)$ can be obtained in the same way. Note that although (22) is used in the energy-efficient CA process for fast and approximate calculation of power consumption, the real power consumption, calculated by instantaneous torques and rotational speeds of motors, is obtained and compared in the simulation results.

IV. Simulation Results and Discussions

In this section, different maneuvers are simulated to verify the SMC and the energy-efficient CA algorithms. The power consumptions and torque distributions are compared with those of the standard CA method. The experimental data for driving efficiencies and regenerative braking efficiencies of in-wheel motors are first described as follows [29].

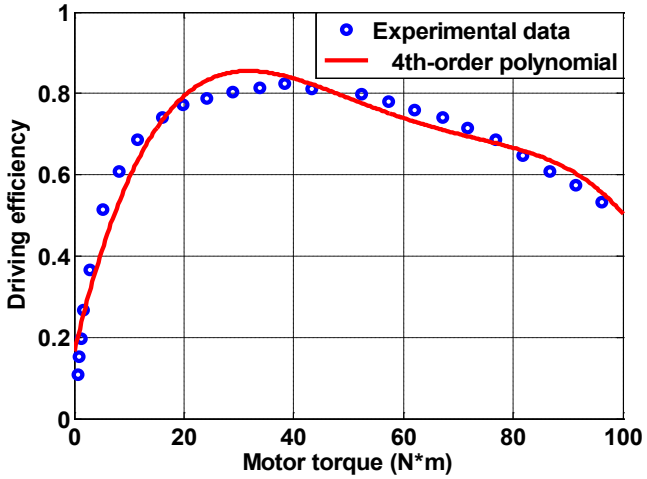

Figure 2. The efficiency curve fitting of an in-wheel BLDC motor based on experimental data.

The driving efficiency of one in-wheel motor $\eta_o(T)$ is expressed by fitting one group of the BLDC motor experimental data at a constant rotational speed in Figure 2.

$$\eta_o(T) = p_1T^4 + p_2T^3 + p_3T^2 + p_4T + p_5, \quad (23)$$

All the parameters p_l, $l = 1, \ldots, 5$ are displayed in Table 1.

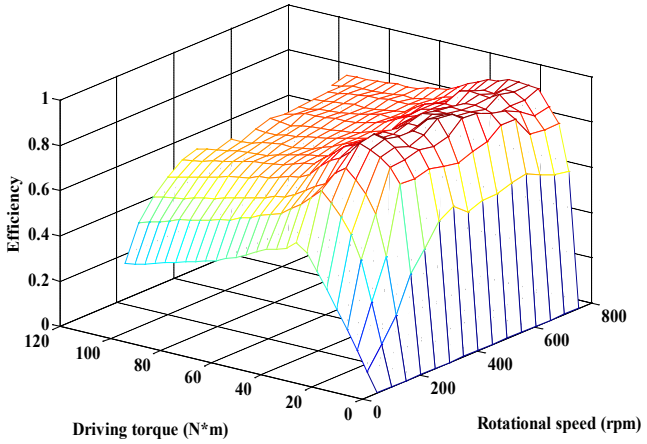

Figure 3. The driving efficiency map of an in-wheel BLDC motor based on experimental data.

Note that although the motor speed also slightly affects the motor efficiency from Figure 3, the efficiency curves are similar within a large range of motor rotational speeds. Moreover, motor rotational speed can be assumed to be a constant at each instantaneous time in energy-efficient CA.

Table 1 Simulation Parameters

Symbol	Values	Symbol	Values
p_1	-7.2888e-5	p'_2	-0.00061109
p_2	1.8023e-5	p'_3	0.034213
p_3	-0.0016099	p'_4	0.010455
p_4	0.057038	K	40000
p_5	0.16446	R_{eff}	0.312
p'_1	3.5227e-6	λ	1e-6

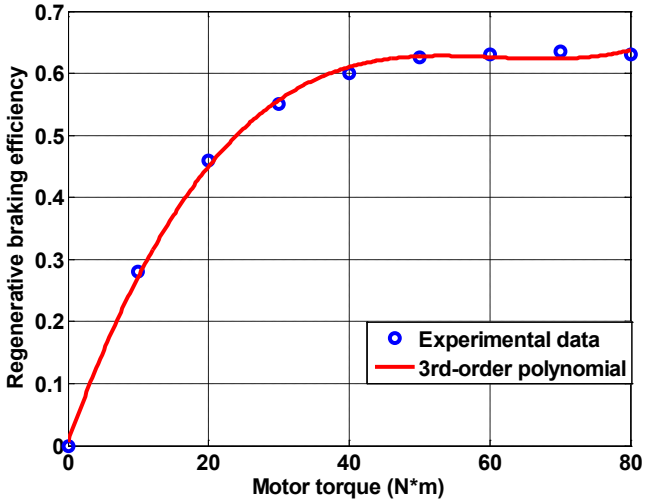

Figure 4. The regenerative braking efficiency curve fitting of an in-wheel BLDC motor based on experimental data.

The regenerative braking efficiency $\eta_i(T')$ is also obtained by fitting one group of the BLDC motor experimental data at a constant rotational speed in Figure 4,

$$\eta_i(T') = p'_1T'^3 + p'_2T'^2 + p'_3T' + p'_4. \quad (24)$$

All the parameters p'_n, $n = 1, \ldots, 4$ are displayed in Table 1.

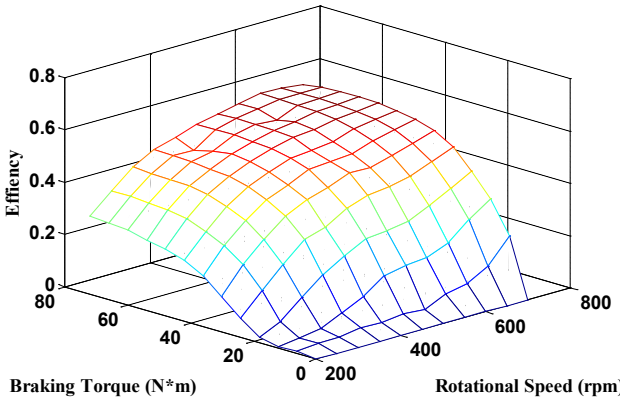

Figure 5. The regenerative braking efficiency map of an in-wheel BLDC motor based on experimental data.

As it is shown in Figure 5, the regenerative braking efficiency curve is lower than the driving efficiency, which is reasonable for a real in-wheel motor. The influence of rotational speed on

efficiency function is neglected because of the same reasons for the driving efficiency case.

Besides the manufacturing processes, different working conditions/environments will make the four in-wheel motors have different efficiencies. Although the differences may not be huge under normal operations, four identical efficiencies in-wheel motors cannot be assumed. Without loss of generality, both driving and regenerative braking efficiencies of the two rear in-wheel motors are scaled by 0.8 respectively to conveniently explain the simulation results.

A combined maneuver of the EGV first contains an acceleration process from 20 km/h to 30 km/h within 2.5 seconds. Then a single lane change (SLC) is commanded at a constant speed from 3.5 second to 6.5 second. Finally, the vehicle speed is decelerated to 20 km/h from 7.5 second to 10 second. The control results and torque distributions by using the dual-mode energy-efficient CA are shown in Figure 6 and Figure 7, respectively.

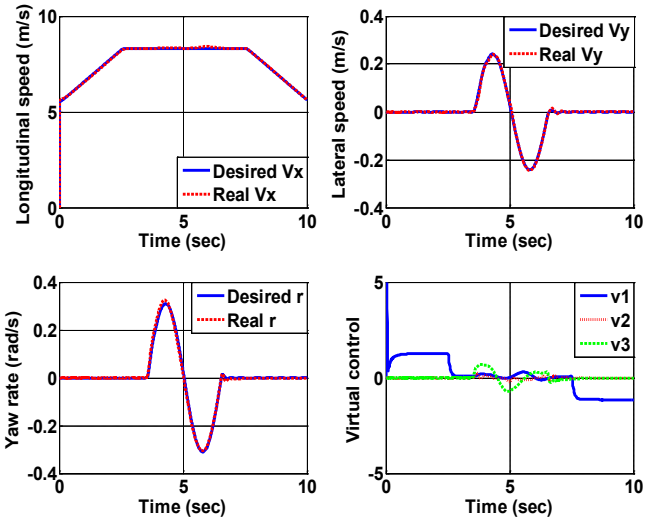

Figure 6. Tracking control effect of planar motions and virtual control for the dual-mode energy-efficient CA.

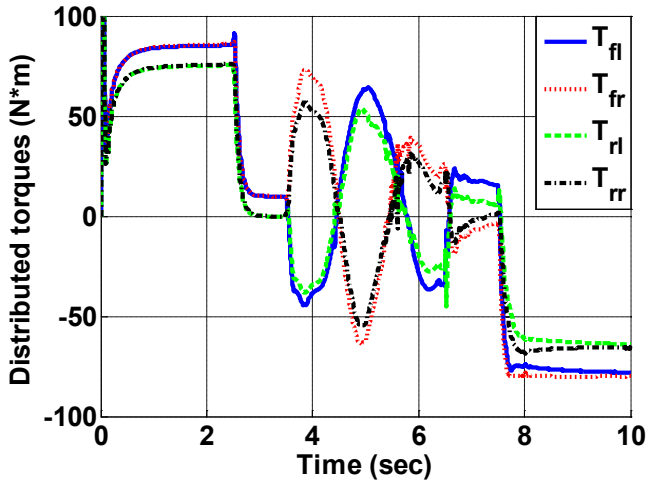

Figure 7. Torque distributions under the dual-mode energy-efficient CA scheme.

From Figure 6, the desired longitudinal, lateral speed and yaw rate are tracked well under SMC. The virtual controls generated by the SMC are distributed to four in-wheel motors by the dual-mode energy-efficient CA to optimize the total power consumptions. As shown in Figure 7, during the acceleration period, the two front high-efficiency motors exert larger driving torques than the two rear low-efficiency motors to reduce the overall power consumptions. In the deceleration period, the front two motors also absorb higher power by exerting larger regenerative braking torques than the rear two motors. During the SLC maneuver, the high-efficiency front motors are always distributed larger driving or braking torques than the low-efficiency rear motors for optimal power consumptions.

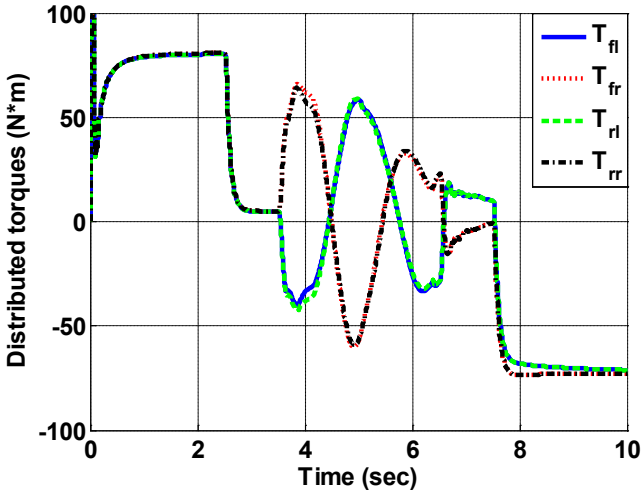

Figure 8. Torque distributions under the standard CA algorithm.

Although the standard CA algorithm can also give good tracking results, similar to the results shown in Figure 6, the torque distributions are just equally distributed to the four or two motors according to the motion requirements, as shown in Figure 8. This torque distribution scheme, which does not consider the different efficiencies of actuators, cannot guarantee the optimal power consumption during the EGV planar motions. Figure 9 clearly displays this point.

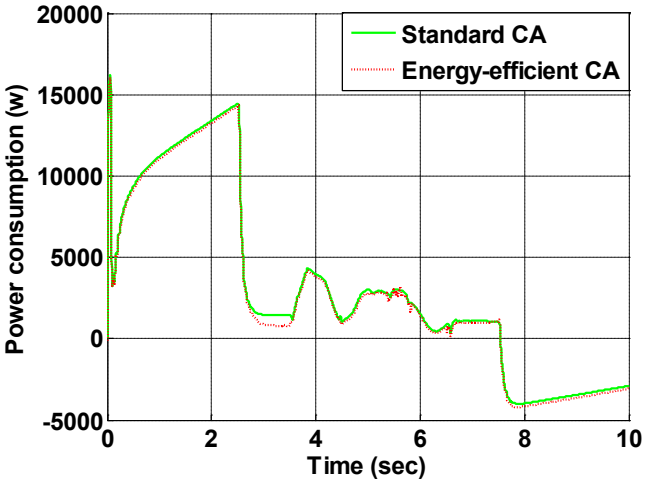

Figure 9. Power consumption comparison between the standard CA and the dual-mode energy-efficient CA.

Figure 9 shows instantaneous power consumptions for both the standard CA and the dual-mode energy-efficient CA during the 10 second maneuver. It is clear to see that the dual-mode energy-efficient CA consumes less power at the

most time period. By integrating the instantaneous power consumptions along time for the 10 seconds, the total energy consumes in the standard CA procedure is 30.568 kJ, which is larger than that consumed in the dual-mode energy-efficient CA case, 29.675 kJ. It is expected that the energy saving will accumulatively increase and become considerable as the travel time is prolonged.

V. Conclusions and Future Work

This paper applies the energy-efficient CA to EGV planar motions actuated by four in-wheel motors. Sliding mode controllers are applied to track the desired longitudinal, lateral and yaw motion of the EGV. Different maneuvers are tested for the comparison between the standard and the energy-efficient CA. In order to optimize the instantaneous power consumptions during planar motion, the energy-efficient CA dictates different torque distributions on each wheel with different efficiencies compared with the standard CA method. Thus, less energy is consumed when the energy-efficient CA is applied.

The future work includes experimental validation and robustness analyses of the control algorithms.

References

[1] S. J. Hallowell and L. R. Ray, "All-Wheel driving using independent torque control of each wheel," *Proceedings of the 2003 American Control Conference*, pp. 2590 – 2595, 2003.

[2] G. S. Buja and M. P. Kazmierkowski, "Direct torque control of PWM inverter-fed AC motors-a survey," *IEEE Transactions on Industrial Electronics*, Vol. 51, No. 4, pp. 744 –757, 2004.

[3] K. M. Rahman, N. R. Patel, T. G. Ward, J. M. Nagashima, F. Caricchi and F. Crescimbini, "Application of direct-drive wheel motor for fuel cell electric and hybrid electric vehicle propulsion system," *IEEE Transactions on Industry Applications*, Vol. 42, No. 5, Sep. 2006.

[4] Y. Hori, "Future vehicle driven by electricity and control-research on four-wheel-motored "UOT electric March II" ," *IEEE Transactions on Industrial Electronics,* Vol. 51, No. 5, pp. 954-962, 2004.

[5] J. Wang and R. G. Longoria, "Coordinated and reconfigurable vehicle dynamics control," *IEEE Transactions on Control Systems Technology*, vol. 17, No. 3, pp. 723 – 732, 2009.

[6] J. Wang and R. G. Longoria, "Combined tire slip and slip angle tracking control for advanced vehicle dynamics control systems," *Proceedings of the 45th IEEE Conference on Decision and Control*, pp.1733 – 1738, 2006.

[7] J. Wang and R. G. Longoria, "Coordinated vehicle dynamics control with control distribution," *Proceedings of American Control Conference*, pp. 5348-5353, 2006.

[8] M. Oppenheimer, D. Doman and M. Bolender, "Control allocation for over-actuated systems," *14th Mediterranean conference on control and automation*, 2006.

[9] T. Fossen and T. Johansen, "A survey of control allocation methods for ships and underwater vehicles," *14th Mediterranean conference on control and automation*, 2006.

[10] M. Benosman, F. Liao, K. Lum and J. L. Wang, "Nonlinear control allocation for non-minimum phase systems," *IEEE Transactions on Control Systems Technology*, Vol. 17, No.2, pp. 394-404, March, 2009.

[11] H. Alwi and C. Edwards, "Fault tolerant control using sliding modes with on-line control allocation," *Automatica*, 44, pp. 1859-1866, 2008.

[12] J. Zheng, W. Su and M. Fu, "Dual-stage actuator control design using a doubly coprime factorization approach," *IEEE/ASME Transactions on Mechatronics*, Vol. 15, No. 1, 2010.

[13] O. J. Sørdalen, "Optimal thrust allocation for marine vessels," *Control Engineering Practice*, Vol. 5, No. 9, pp. 1223-1231, 1997.

[14] M. Bodson, "Evaluation of optimization methods for control allocation," *Journal of Guidance, Control, and Dynamics*, Vol. 25, No.4, pp. 703-711, 2002.

[15] D. B. Doman, B. J. Gamble and A. D. Ngo, "Quantized control allocation of reaction control jets and aerodynamic control surfaces," *Journal of Guidance, Control, and Dynamics*, Vol. 32, No.1, pp. 13-24, 2009.

[16] M. Gerard and M. Verhaegen, "Global and local chassis control based on load sensing," *Proceedings of the 2009 American Control Conference*, pp. 677-682, June, 2009.

[17] J. H. Plumlee, D. M. Bevly and A. S. Hodel, "Control of a ground vehicle using quadratic programming based control allocation techniques," *Proceedings of the 2004 American Control Conference*, pp. 4704-4709, Boston, 2004.

[18] J. Wang, J. M. Solis and R. G. Longoria, "On the control allocation for coordinated ground vehicle dynamics control systems," *Proceedings of the 2007 American Control Conference*, pp. 5724-5729, July, 2007.

[19] J. Tjønnås and T. A. Johansen, "Stabilization of automotive vehicles using active steering and adaptive brake control allocation," *IEEE Transactions on Control Systems Technology*, Vol. 18, No. 3, pp. 545-558, May, 2010.

[20] K. Tagesson, P. Sundström, L. Laine and N. Dela, "Real-time performance of control allocation for actuator coordination in heavy vehicles," *IEEE Intelligent Vehicles Symposium,* pp: 685 – 690, 2009.

[21] Y. Chen and J. Wang, "Energy-efficient control allocation for over-actuated systems with electric vehicle applications," *Proceedings of the 2010 ASME Dynamic Systems and Control Conference*, Boston, 2010.

[22] J. Nocedal and S. Wright, "Numerical Optimization," Springer, 2006.

[23] H. B. Pacejka and E. Bakker, "Magic formula tyre model," *Vehicle System Dynamics*, Vol. 21, No. Suppl: Tyre Models for Vehicle Dynamics Analysis, pp. 1-18, 1993.

[24] J. Y. Wong, *Theory of Ground Vehicles*. New Jersey: John Wiley & Sons, 2008.

[25] R. Rajamani, *Vehicle Dynamics and Control*, Springer, 2006.

[26] J.-J. E. Slotine and W. Li, *Applied Nonlinear Control*. Prentice Hall, 1991.

[27] V. Utkin, J. Guldner and J. Shi, *Sliding Mode Control in Electro-Mechanical Systems*. CRC Press, 2nd edition. 2009.

[28] R. N. Jazar, "Vehicle Dynamics: Theory and Application," Springer, 2009.

[29] R. Wang, Y. Chen, D. Feng, X. Huang, and J. Wang, "Development and Performance Characterization of an Electric Ground Vehicle with Independently Actuated In Wheel Motors," *Journal of Power Sources*, Vol. 196, No 8, pp. 3962-3971, 2011.

[30] Y. Chen and J. Wang, "Adaptive Vehicle Speed Control with Input Injections for Longitudinal Motion Independent Road Frictional Condition Estimation," *IEEE Transactions on Vehicular Technology*, Vol. 60, No. 3, pp. 839 - 848, 2011.